Title

Depth-resolved variations in visibility of retinal nerve fibre bundles across the retina in enface OCT images of healthy eyes

Authors

Riccardo Cheloni & Jonathan Denniss

Affiliations

School of Optometry and Vision Science, University of Bradford, UK

Corresponding author

Jonathan Denniss, j.denniss@bradford.ac.uk

Abstract

Purpose

Recent developments in optical coherence tomography (OCT) technology enable direct enface visualisation of retinal nerve fibre bundle (RNFB) loss in glaucoma, however, the optimum depth at which to visualise RNFBs across the retina is unknown. We aimed to evaluate the range of depths and optimum depth at which RNFBs can be visualised across the retina in healthy eyes.

Methods

The central ±25° retina of 10 healthy eyes from 10 people aged 57-75y (median 68.5y) were imaged with spectral domain OCT. Slab images of maximum axial resolution (4μm) containing depth-resolved attenuation coefficients were extracted from 0 to 193.5μm below the inner limiting membrane (ILM). Bundle visibility within 10 regions of a superimposed grid was assessed subjectively by trained optometrists (n=8), according to written instructions. Anterior and posterior limits of RNFB visibility and depth of best visibility were identified for each grid sector. Effects of retinal location and individual eye on RNFB visibility were explored using linear mixed modelling with likelihood ratio tests. Intraclass correlation coefficient (ICC) was used to measure overall agreement and repeatability of grading. Spearman's correlation was used to measure correlation between depth range of visible RNFBs and retinal nerve fibre layer thickness (RNFLT).

Results

Retinal location and individual eye affected anterior limit of visibility ($\chi^2_{(9)}$ = 58.6 & 60.5, both p<0.0001), but none of the differences exceeded instrument resolution making anterior limit consistent across the retina and different eyes. Greater differences were observed in the posterior limit of visibility across retinal areas ($\chi^2_{(9)}$ = 1671.1, p<0.0001) and different eyes ($\chi^2_{(9)}$ = 88.7, p<0.0001). Optimal depth for visualisation of RNFBs was around 20μm below the ILM in most regions. It varied slightly with retinal location ($\chi^2_{(8)}$ = 58.8, p<0.0001), but it was not affected by individual eye ($\chi^2_{(9)}$ = 10.7, p=0.29). RNFB visibility showed good agreement between graders (ICC 0.89, 95%CI 0.87-0.91), and excellent repeatability (ICC 0.96 to 0.99). Depth range of visible RNFBs was highly correlated with RNFLT (ρ = 0.9, 95%CI: 0.86-0.95).

Conclusions

The range of depths with visible RNFBs varies markedly across the healthy retina, consistently with RNFLT. To extract all RNFB information consistently across the retina, slab properties should account for differences across retinal locations and between individual eyes.

Introduction

Optical coherence tomography (OCT) is now widely available in glaucoma clinics, being used to objectively quantify structural changes to the retina and optic nerve head.[1,2] Nevertheless, glaucoma detection, diagnosis and monitoring are still imperfect.[3-5] As such, glaucoma and its progression must currently be confirmed across multiple tests, resulting in delayed treatment and increased socio-economic burden.[6] There remains, therefore, considerable interest in improved identification of glaucomatous damage, which has led to consideration of retinal nerve fibre layer (RNFL) reflectance information from enface OCT images.[7,8]

Retinal nerve fibre bundles (RNFBs) are highly reflective compared to other retinal structures because of the ordered structure of ganglion cell axons' cytoskeleton.[9] Recent OCT devices allow us to qualitatively explore reflectance in enface images of the RNFL.[10-12] Enface analysis is often accomplished with volumetric scans by collapsing the pixel intensity of each A-scan over a certain range of depths into a 2D image. The result is a single transverse retinal section, or slab, frequently derived from a fixed retinal thickness (often 50μm) beginning anteriorly from the inner limiting membrane (ILM).[11,12] In these images, glaucomatous defects appear as regions of impaired reflectance, often in typical arcuate or wedge shapes as well as more generalised loss. Defects are likely to be induced from a combination of primary loss of reflectivity, caused by cytoskeletal disruption,[9,13] and thinning of the RNFL which leads to the inclusion of deeper hypo-reflective retinal layers in the slab.[11] Previous studies of enface OCT imaging in glaucoma showed a strong correlation with circumpapillary RNFL defects,[10] and excellent agreement between residual RNFBs and preserved visual function in the macula.[12,14]

It has been suggested that disruption of RNFB reflectivity may be measureable earlier than RNFL thinning in glaucoma,[8,15] making this approach encouraging for earlier identification of defects. Further, clinicians are encouraged to confirm a suspected structural lesion in the functional domain to increase confidence in diagnosis.[16-19] Enface images offer the opportunity to relate structure and function without use of structure-function maps, thought to represent an additional source of noise in this relationship.[20] Indeed, newer perimetric strategies that aim to incorporate structural information for greater efficiency,[21-23] or that assess specific regions of interest in greater detail,[24-26] may be facilitated by enface imaging.

Although the use of enface OCT images is promising, current understanding of the arrangement of visible RNFBs in healthy eyes is lacking. Understanding of the normal appearance of RNFBs in enface OCT images is important in the future development of objective methods for detecting glaucomatous defects in these images. For instance, it is unclear how RNFB visibility in enface OCT images varies across the healthy retina and between individual eyes. It is, therefore, also unclear what depths should be considered to capture a consistent portion of the RNFL through the retina. Using a fixed thickness slab to examine portions of the retina with varying morphology may be expected to lead to an uneven composition whereby some areas contain RNFL only, whilst some also include deeper retinal layers with different reflectivity. This would most likely result in different appearance and detectability of glaucoma defects across the retina.[10] Additionally, since there may be situations where it is desirable to use a single slab thickness across the retina, the axial placement of this slab within the thicker regions of RNFL may affect the detectability of glaucomatous defects. It may therefore be advantageous to know whether there is an optimum depth for visualisation of RNFBs and how this varies across the retina. Looking for glaucomatous defects at this depth may achieve higher specificity than other depths if it results in a lower chance of misidentifying normal variation as a defect.

In this study we aimed to identify the range of depths and the optimal depth for the subjective visualisation of RNFBs across different retinal regions in eyes of healthy adults. Further, we assessed the agreement between- and repeatability within- clinicians in determining RNFB visibility. Since RNFL thickness varies across the healthy retina,[27] we expected RNFBs to be visible over a range of depths that varies across the retina and between individual eyes. The results contribute to a preliminary understanding of the three dimensional configuration of RNFBs in healthy eyes as viewed subjectively in enface OCT images, identifying the depths that future automated image analysis methods should consider to consistently assess the RNFL.

Methods

Participants

Healthy volunteers aged over 50 years were recruited for imaging. We targeted older adults to include an age range relevant to primary open angle glaucoma.[28] One eye per participant was included. Participants were eligible if they had visual acuity ≤0.20

logMAR (6/9.5 Snellen) measured at 6m with appropriate refractive correction using an electronic logMAR chart. Further inclusion criteria were clear optical media and normal visual field (Humphrey Field Analyser III SITA standard, www.zeiss.com/meditec), as defined by normal Mean Deviation (P > 0.05), Glaucoma Hemifield Test within normal limits and absence of three contiguous non-edge points with P<5% on the Pattern Deviation plot. Participants were excluded if they had any condition affecting their eyes or visual system, or intraocular pressure >21mmHg in either eye or between eye difference >4mmHg by Goldmann applanation tonometry. Written informed consent was given by each participant. Ethical approval was obtained from the National Health Service Research Ethics Service and the study adhered to the Declaration of Helsinki.

OCT imaging and processing

Multiple high density high-speed scans encompassing the central ±25º of the retina were acquired with Spectralis OCT (www.heidelbergengineering.com). Seven volume scans comprising 30µm-separated B-scans (9.65 B-scans per degree) were captured in different positions of gaze (Figure 1). Measurement noise was reduced by the use of built-in automated retinal tracking to average 16 B-scans per scan location. The orientation of B-scans was adjusted to yield high image resolution in a shorter time (Figure 1). Pupils were dilated only if inadequate scan quality was achieved in physiological conditions (i.e., below 25db as suggested by the manufacturer and elsewhere[29]). All images were acquired with signal to noise ratio above 20dB as per the manufacturer's instructions. Traditional OCT imaging of the optic nerve head (ONH) was also performed, including a circle B-scan (3.5mm diameter) around the ONH that provided the mean circumpapillary RNFL (cpRNFL) thickness as automatically computed by Spectralis built-in software.
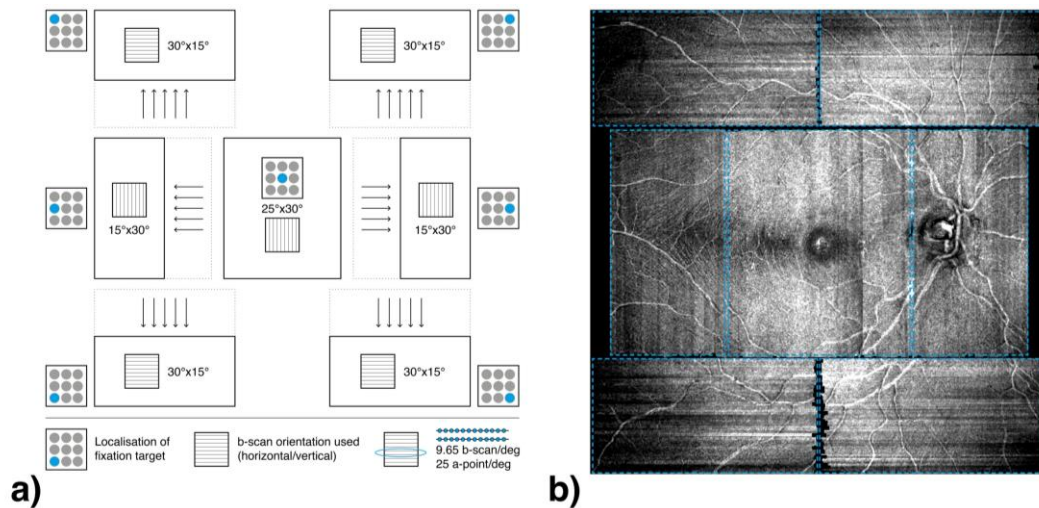
Figure 1: (a) The wide field OCT acquisition protocol comprised of 7 volume scans (black boxes) shown within the acquisition window (dashed boxes) at each scan location. Scan dimensions and orientation are shown for every location. Arrows indicate the movement of scan positions from the manufacturer's default positions. The level of overlap between different scans was considerable between superior scans and inferior scans as well as between superior/inferior and central scans. The overlap between central scans was instead marginal. (b) Example of the resulting attenuation coefficients pseudo-montage for one eye 20µm below the inner limiting membrane. Individual volume scan positions are shown by the blue boxes.

For each eye, we extracted 50 single-pixel thick slabs containing depth-resolved attenuation coefficients[30] encompassing the volume from 0 to 193.5µm below the ILM. Each slab represents a 3.87µm thick slab through the retina, corresponding to the instrument's digital axial resolution. The greatest depth explored with this method (193.5µm) was selected in order to include the maximum expected cpRNFL thickness for a 50 year old healthy individual. As proposed elsewhere,[10] we extracted attenuation coefficients instead of the raw intensity of each pixel using equations 17 and 18 in Vermeer et al.[30] Attenuation coefficients are purported to describe how quickly incident light is attenuated when passing through the retinal portion of interest irrespective of the amount of light received.[31] Although attenuation coefficients were originally developed to minimise shadowing effects of blood vessels on underlying tissue, they should also minimise reflectance artefacts from media opacity and poor quality B-scans.[10] Images for each retinal area and depth were converted from the raw output of the Spectralis to attenuation coefficients using custom software written in *R* (version 3.6.3),[32] prior to exporting to Matlab for further processing (Version 9.6.0, The MathWorks Inc, Natick, Massachusetts).

At each depth, for each individual eye, we collated the 7 arrays together into a single pseudo-montage image (Figure 1b). Because of some extent of overlap between

individual scans, this method resulted in partial duplication of information from certain retinal areas that was accounted for at later stages (see below). Then, we applied a smoothing filter (3x3 Wiener filter) to all images to reduce noise. Subsequently, a 100x50 pixel rectangle was extracted from the raphe area of the composite image 35μm below the ILM of each participant and a value 30% below the median pixel value within this rectangle was computed as 'background'. The background value is, therefore, computed from an area expected to be lacking any RNFBs. This was used as a reference to reset the lower limit of the image.[10] A two-step thresholding process was then applied. First, the background value was subtracted from all pixels of all slabs, with values falling below 0 being clipped to 0. Then, for each participant the median of the 99th percentiles of all 50 slabs was computed and used to normalise each slab by division, with values above 1 being clipped to 1. This process left all pixel values within a 0 to 1 range, before 8 bit images were extracted for display in the grading task.

Grading task

Subjective visibility of RNFBs was rated over 10 retinal regions of interest, each approximately consisting of a 15x15° square with the exception of the macular area that was further split into temporal and nasal regions (Figure 2). To account for inter-subject anatomical variability,[33,34] the central row of the grid was tilted to follow each individual's fovea-disc and fovea-raphe angles (Figure 2). The number of retinal regions delimited represented a trade-off between resolution and the time required to complete the task within manageable limits. To minimise potential bias from duplication of information, overlapping areas from different scans were obscured and graders were instructed to ignore those areas during the task (Figure 2). An example of the presentation file presented to clinicians is available as supporting material (Supplementary material 1).
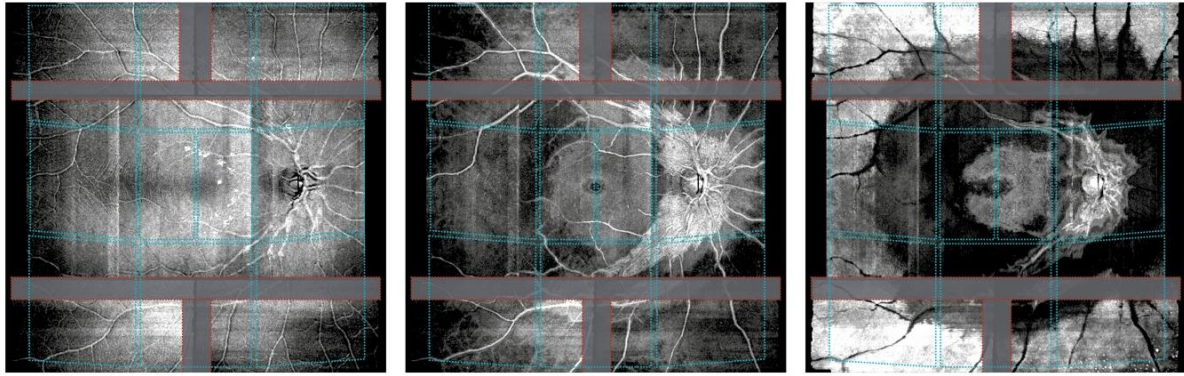
Figure 2: Example of the grid (blue lines) superimposed onto 3 of the 50 pseudo-montaged slab images for one eye, delimiting the regions of interest in the retina. Grey patches within red dashed bounding lines indicate the overlapping areas that graders were instructed to ignore. From left to right, the images correspond to 12µm, 93µm and 186µm below the ILM, showing how the visible presence of RNFBs changes moving away from the ILM. At 12µm below the ILM, RNFBs are visible almost throughout the whole retina, with exception of the raphe, the fovea and peripheral portions of the inferior temporal, nasal and superior temporal regions. The reduction of reflectivity in these areas can be interpreted as absence of RNFBs. At 93µm below the ILM, RNFBs are present only in the ONH region, with arcuate wedges of RNFBs in the inferior and superior central retina following the vascular arcades. Lastly, at 186µm below the ILM, it is possible to appreciate hyper-reflectivity of the retinal pigment epithelium in almost all peripheral regions and the macula, whereas only a few visible bundles are present around the ONH.

Images were displayed in randomised order on a MacBook Pro 13" (2017 version, Apple Inc, USA) under standardised lighting conditions. Before performing the task, all graders were provided with the same written instructions (Supplementary material 2), which included information on characteristic appearance of RNFBs, visible artefacts and potential confounders (e.g. putative glial alteration[35]). Subsequently, they were allowed to scroll through the images for a given eye unlimited times and without a time limit. The following subjective judgements were collected for each region of each imaged eye:

i) Boundaries of RNFB visibility: The first depth below the ILM at which RNFBs become visible in that specific region (anterior limit – µm) and the depth below the ILM at which RNFBs are last visible in that specific region (posterior limit – µm). Graders were instructed to consider RNFBs to be present when 25% or more of the region was occupied.

ii) Best visibility of RNFBs: The depth of greatest RNFB visibility (µm) according to features such as intensity and sharpness while ignoring the proportion of the region occupied from RNFBs. Since the best visibility value aims to identify a single pixel depth for optimum observation of bundles, in the case of equal visibility of RNFBs across multiple depths graders were invited to report '*none*'.

Eight optometrists including the two authors (median age 29.5, range 26 to 41; median years since qualification 7, range 2 to 16) completed the grading task. The optometrists had varying level of post-qualification training (4 out of 8 had undertaken specific training in glaucoma), but apart from the two authors they were all naïve to enface OCT images showing reflectivity details of healthy retinae. All were pre-presbyopic, with self-reported normal vision, and were invited to perform the task with their habitual refractive correction. To assess repeatability of the gradings, on a subgroup of 2 graders, the task was repeated 3 times on 3 randomly selected eyes and with no information regarding previous grades available. Repeated measures were taken 1 week apart.

Data analysis

All data were anonymised before analysis in the open-source environment *R*.[32] The effects of retinal region and individual eye on anterior limit of visibility, posterior limit of visibility and best depth for RNFB visibility were explored with linear mixed modelling using the *R* package *lme4*.[36] Means were computed to summarise ratings from all graders at each region of each eye. For greater robustness of results, best visibility analysis was limited to cases where the proportion of 'none' ratings was below 30%. The first model tested whether retinal region affected boundaries of visible bundles and best visibility, accounting for random effects of eye and grader. This model had the form:

$$y \sim 1 + region + (1|eye) + (1|grader) + \varepsilon \qquad (1)$$

where y signifies the measure of interest (e.g. best visibility depth), 1 signifies the intercept and ε signifies random error. Second, effects of individual eye on RNFB visibility were tested accounting for different retinal regions and graders using a model of the form:

$$y \sim 1 + eye + (1|region) + (1|grader) + \varepsilon \qquad (2)$$

whose symbols are as defined for equation 1. Chi-squared likelihood ratio tests were used to assess statistical significance of variables, with $p<0.05$ considered significant. Where relevant, post-hoc analysis was performed to test pairwise differences, adjusting for multiple comparisons with the Tukey method.

To explore overall agreement between graders and repeatability within graders, we computed intraclass correlation coefficients (ICC), according to Shrout and Fleiss,[37] using the *R* package *psyc*.[38] ICC classes ICC(2,1) and ICC(3,1) for a single rating were used to estimate reliability and repeatability respectively. ICC is strongly influenced by the variance of the sample,[39] thereby not allowing for comparison among subgroups of data with inconsistent variances. Hence, to further evaluate variability between graders for different tasks and retinal regions we also computed the central 90% range width (difference between 5th and 95th percentiles) of ratings at each region of each image. This was done for ratings of anterior limit, posterior limit and best visibility. We refer to this measure as between-grader variability henceforth. As above, linear mixed models were used to explore the effects of retinal region and individual task on agreement. The model testing the effect of retinal region on between-grader variability included task and individual eye as random effects and had the form:

$$variability \sim 1 + region + (1|task) + (1|eye) + \varepsilon \qquad (3)$$

where 1 signifies the intercept and ε signifies random error. Effects of task were assessed accounting for retinal region and individual eye:

$$variability \sim 1 + task + (1|region) + (1|eye) + \varepsilon \qquad (4)$$

where terms are as per equation 3.

We also sought validation that the object of the subjective grading task was actually the visibility of RNFBs, and not some other retinal image feature. We therefore evaluated correlation (Spearman's ρ) between thickness of visible RNFBs, computed as the axial distance (μm) between the subjectively-defined anterior and posterior limits of visible RNFBs, and mean RNFL thickness in the corresponding region. To this end, RNFL thickness data as automatically segmented by Spectralis OCT were extracted from the wide-field scans and the mean thickness was computed along the same grid adopted for the grading task. Lastly, correlation between thickness of visible bundles and between-grader variability was tested.

Following a previous study,[40] we calculated that the selected combination of number of graders, images and repetition should produce 95% confidence intervals (CI) within

0.1 for the agreement ICC for any value of ICC, and within 0.1 for repeatability ICC >0.79.

Results

Images from 10 eyes from 10 healthy participants were included in the study (5 females, 9 Caucasian, median age 68.5 years, range 57 to 75), whose demographic and clinical details are reported in Table 1. The grading task required a median total of 73 minutes (range 51 to 144 minutes).

Table 1: *Demographics and RNFL parameters for the 10 imaged eyes.*

Participant	Eye	Age (y)	Mean cpRNFL thickness (μm)	Mean thickness of visible RNFBs (μm)
1	R	57	92	38
2	R	63	108	48
3	R	66	90	43
4	L	72	97	42
5	R	69	111	50
6	R	73	98	43
7	L	67	99	48
8	R	68	96	42
9	L	75	78	38
10	R	73	103	46

The grand mean and (±) standard deviation for anterior limit of visibility was 9.9±0.8μm (range 8.8±1.5μm for superior nasal region to 11.3±1.5μm for ONH region) and the grand mean for posterior limit of visibility was 53.7±30.6μm (range 28.1±1.2μm for raphe region to 131.6±13.7μm for ONH region). As shown in Figure 3, retinal region affected the anterior limit of RNFB visibility ($\chi^2_{(9)}$ = 58.6, p<0.0001), and the greatest difference was found between the optic disc region and the superior nasal region (2.5μm, p<0.0001). Nonetheless, this difference was below the instrument's digital axial resolution, and is therefore not clinically significant. Similarly, there were

significant differences between individual eyes in anterior limit of RNFB visibility ($\chi^2_{(9)}$ = 60.5, p<0.0001), but again these differences did not exceed digital axial resolution so are not clinically significant (greatest pairwise difference: 2.5µm, p<0.0001). Conversely, differences in posterior limit of RNFB visibility across both retinal regions ($\chi^2_{(9)}$ = 1671.1, p<0.0001) and individual eyes ($\chi^2_{(9)}$ = 88.7, p<0.0001) were both statistically and clinically significant (mean difference between retinal regions 31.1µm, range 0.3 to 103.5 µm; mean difference between individual eyes 4.6µm, range 0.2 to 12µm). Mean limits of RNFBs visibility for individual regions are reported in Figure 3.
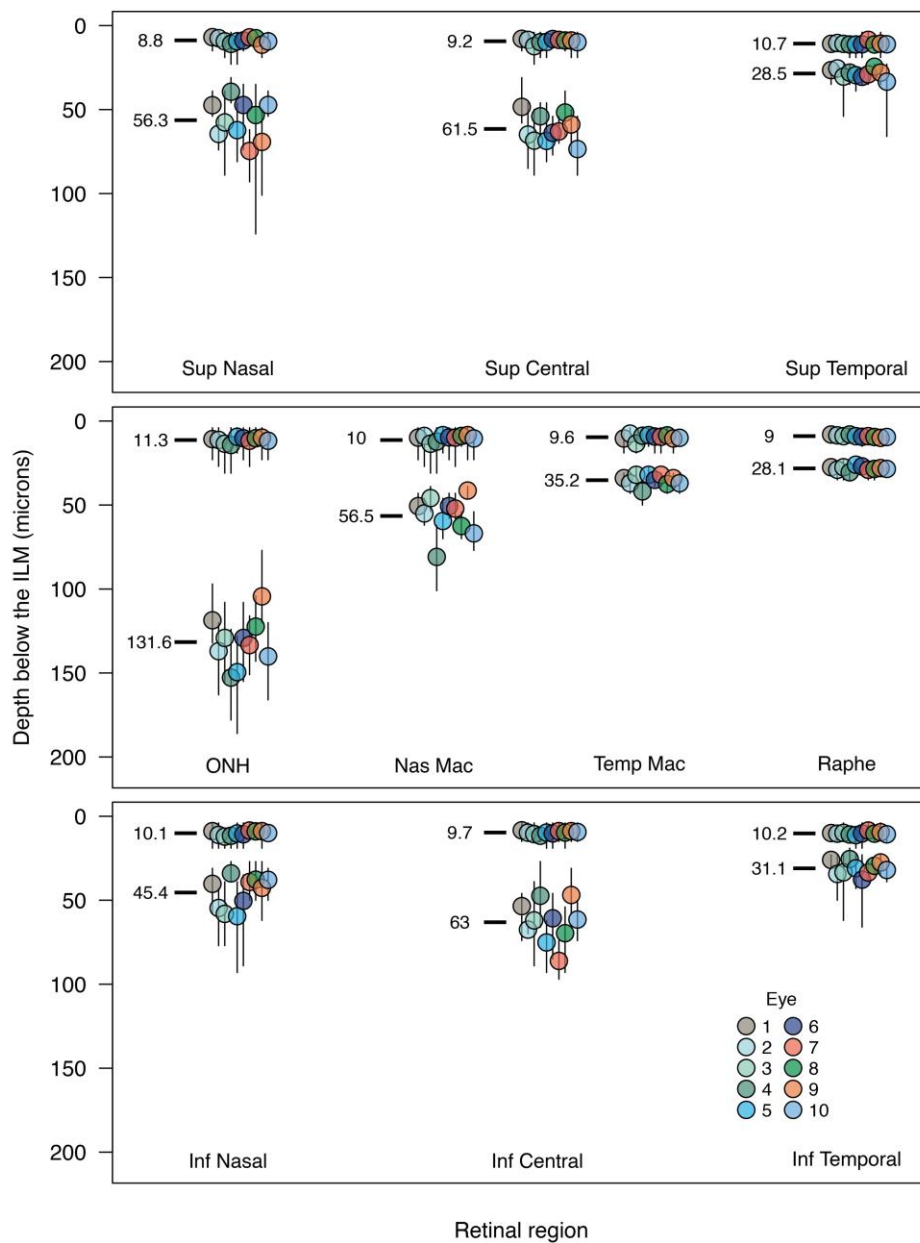

Figure 3: Anterior and posterior limits of RNFB visibility (µm) at different retinal regions. The top, middle and lower panels correspond to the superior, central and inferior retina respectively. Points and error bars show respectively the mean and range of all ratings for each of the 10 individual eyes. Black lines and numbers on the left of each cluster of points show the group mean limit of visibility

across all eyes. Points are color-coded according to individual eyes numbered as in Table 1. ILM=inner limiting membrane, ONH=optic nerve head, Sup=superior, Inf=inferior, Nas=nasal, Temp=temporal, Mac=macula.

As shown in Figure 4, the optimum depth for best RNFB visibility was affected by retinal region ($\chi^2_{(8)}$ = 58.8, p<0.0001). The rate of ungradable judgements for each retinal region is shown in Figure 4 and it was within 30% for most of retinal regions. In the ONH region, 40% of time graders could not identify a single depth with best visibility of bundles. For greater robustness, the region was therefore excluded from this analysis. The grand mean for best RNFBs visibility was 20.3±1.9µm (range 17.4±1.3µm for raphe region to 22.8±2.0µm for the nasal macula), whereas mean limits for individual regions are reported in Figure 4. Pairwise analysis showed most of the significant differences to be just above the instrument's digital axial resolution (greatest difference between nasal macula and raphe regions, 5.4µm, p<0.0001). In contrast, differences in optimum depth for best RNFB visibility between eyes were not significant ($\chi^2_{(9)}$ = 10.7, p=0.29).
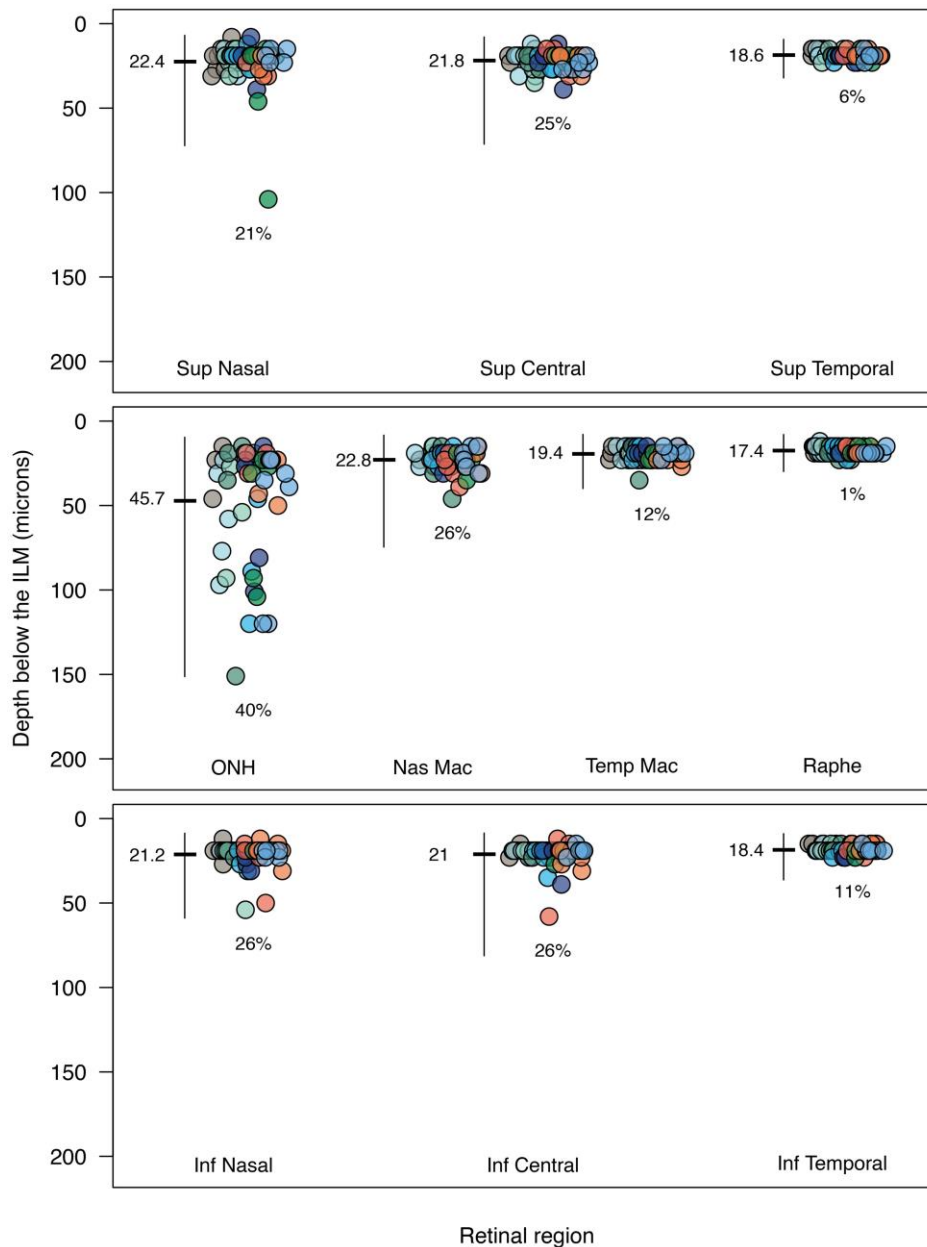
Figure 4: Optimum depth for best RNFB visibility at different retinal regions. Individual points show individual graders' ratings of individual eyes with eyes colour-coded as in Figure 3. Horizontal black bars and numbers show mean ratings across all graders and eyes. Vertical bars indicate depths where RNFBs were visible (5th and 95th percentiles of overall anterior and posterior limit of visibility respectively). Percentage of ungradable ratings (no single best depth identified) is shown for each location. Panel arrangement and abbreviations are as in Figure 3.

Overall we found good agreement between graders' ratings of RNFB visibility (ICC(2,1) = 0.89, 95%CI: 0.87-0.91). Similarly, graders' estimates were highly repeatable (grader 1, ICC(3,1) = 0.96, 95%CI: 0.95-0.97; grader 2, ICC(3,1) = 0.99, 95%CI: 0.98-0.99). Between-grader variability is shown in Figure 5. Retinal region had a significant effect on between-grader variability ($\chi^2_{(9)}$ = 158.3, p<0.0001), with greatest differences found between the ONH region and other retinal regions (max

difference: ONH/raphe=35.8µm, p<0.0001). Ratings appeared progressively more variable in nasal regions compared to temporal regions (superior nasal-superior temporal: 11.74µm, p=0.003; ONH-raphe: 35.76µm, p<0.0001; and inferior nasal-inferior temporal: 7.04µm, p=0.33). Similarly, task significantly affected between-grader variability ($\chi^2_{(2)}$ = 38.5, p<0.0001), with the identification of the posterior limit of RNFBs visibility being the most variable (mean between-grader variability 20.7µm) compared to anterior limit (10.3µm) and best visibility (14.9µm). Differences in between-grader variability among tasks were all statistically significant once adjusted for multiple comparisons (anterior and best: -4.63µm, p=0.012; anterior and posterior: -10.44µm, p<0.0001; best and posterior: -5.81µm, p=0.001).
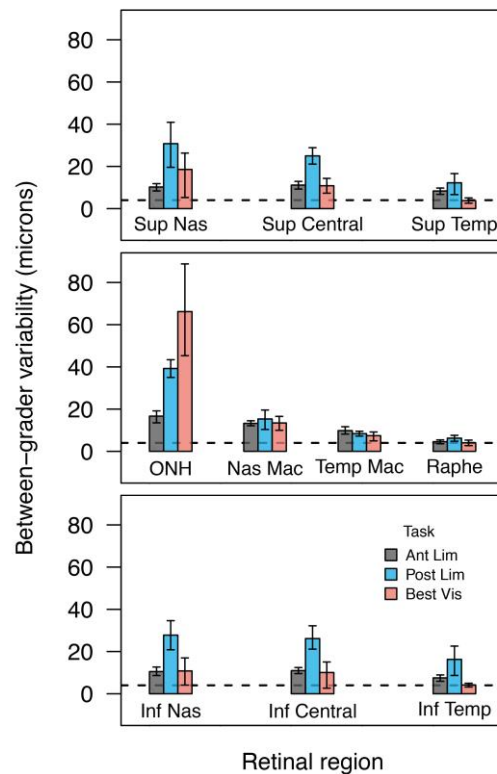

Figure 5: Between-grader variability in ratings for each task and retinal region. Between-grader variability was computed as the central 90% range width (difference between 5th and 95th percentiles) of ratings at each region of each image. Panel arrangement and abbreviations as in Figure 3. Error bars represent bootstrap 95% confidence intervals. Horizontal dashed lines indicate the instrument's digital axial resolution.

Figure 6 shows the strong correlation between thickness of visible RNFBs (axial distance between anterior and posterior limits of visibility) and RNFL thickness as measured by the Spectralis OCT (Spearman's ρ: 0.9, 95%CI: 0.85-0.93, p<0.0001). For all tasks, consistency in ratings between clinicians showed inverse correlation with

thickness of visible RNFBs (greater consistency was apparent in thinner areas, Spearman's ρ: 0.66, 95%CI: 0.58-0.72, p<0.0001).
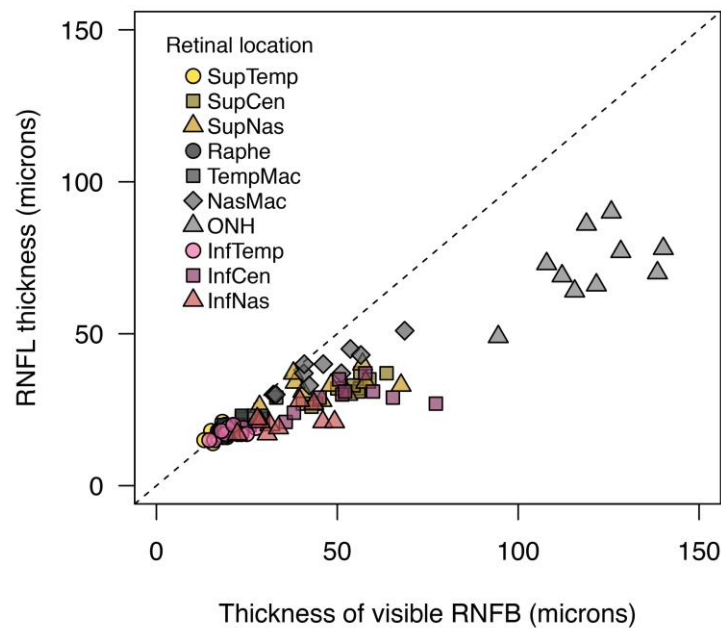

Figure 6: Thickness of visible retinal nerve fibre bundles (RNFB) vs. mean RNFL thickness in the corresponding retinal sector. Points are coded according to the retinal location as shown in the key. The dashed line represents a 1:1 relationship.

Discussion

The detection of RNFB abnormalities in enface OCT images is a promising approach to diagnose and monitor glaucoma, complementary to existing morphological examination.[10-12,41,42] Yet, clinical use of this information is limited by coarse understanding of the normal appearance of RNFBs at different depths and a lack of methods to objectively define defects. For both reliable imaging and defect definition, ideally achieved by objective and quantitative methods, we require adequate understanding of configuration in healthy eyes, including the depths at which RNFBs are visible across the retina. Such information was not previously available and therefore was the objective of this investigation.

Our data suggest that the first depth below the ILM at which bundles become visible is consistent throughout the retina as well as in different eyes. Conversely, retinal region and between-eye factors had statistically and clinically significant effects on the posterior limit of visibility, requiring consideration when extracting enface slab images. Notably, pairwise analysis showed that not all retinal regions had a different posterior limit of visibility, identifying some with a similar range of depths of visible bundles

(Figure 7a). Optimum depth for best bundle visibility varied with retinal region but was similar across different eyes. The number of ungradable ratings changed across the retina, exceeding the 30% in the ONH region where optimal visibility was also found at a wider range of depths. Among the remaining retinal regions, best depth was often found at around 20μm below the ILM (mean 20.3μm, range 17.4 to 22.8), and although pairwise differences were statistically significant for a few regions (Figure 7b), they were close to the OCT instrument's digital axial resolution (greatest difference: 5.4μm, p<0.0001), meaning that depth differences were 1-2 pixels at most. This index provides a single depth at which visualisation of RNFBs appeared optimal across the retinae of the studied eyes, and at which any associated enhanced value in detecting defects could be further explored in future studies of glaucoma.
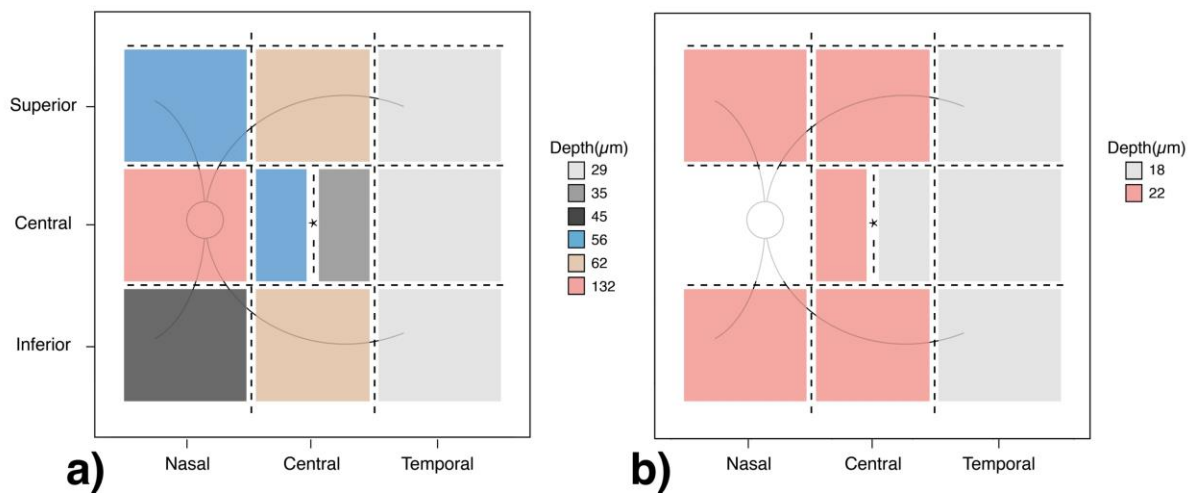

Figure 7: Schematic representations of pairwise differences between retinal regions for: (a) posterior limit of visibility; and (b) the optimum depth of visibility. Retinal regions are coloured differently in cases of a statistically significant difference exceeding the instrument digital axial resolution (4μm). This analysis identified 6 and 2 macro-regions for the posterior limit and best visibility respectively. The anterior limit of visibility was omitted since differences between retinal regions were all below 4μm.

Overall, we found good repeatability and conformity between graders for identification of RNFB visibility, supporting findings from a recent study where raters consistently reported the presence or absence of bundles.[14] A more detailed analysis of between-grader variability showed greater variability for best visibility and posterior limit of visibility compared to anterior limit of visibility. Further, we found between-grader variability to change with retinal region, becoming progressively greater in nasal regions, where the RNFL thickness is known to increase.[27,43] It is possible that the presence of visible bundles at an increased range of depths led to this increase in variability between-graders. This hypothesis is also supported by the correlation

between between-grader variability and the thickness of visible bundles in the corresponding region. Still, even though clinicians were more variable in certain retinal regions, the overall high to excellent ICCs support the validity of the visible ranges identified.

No previous studies have characterised RNFB visibility of the central ±25° of healthy retinae. Additionally, our analysis is the first to consider single slabs of the maximum axial resolution as the unit of assessment of RNFB reflectivity. Most previous work has collapsed a volume of a fixed retinal thickness into a single 2D slab image to explore glaucomatous defects.[10-12,14] Among the earliest, Hood et al[11] assessed loss of reflectivity of the central retina using fixed thickness slabs obtained by averaging intensity values up to 52μm below the ILM (roughly corresponding to the average of 14 slabs in our study). Their axial depth was a compromise between a small thickness – able to show local changes of reflectivity – and a large enough number of pixels to reduce noise. The authors acknowledged that in certain damaged regions the RNFL might have been as thin as 20-30μm, leading to the inclusion of deeper hypo-reflective layers (i.e., ganglion cell and inner plexiform layers). Their analysis may also have been limited by the incomplete capture of the full depth of RNFBs in some regions. In a larger study, Ashimatey et al[10] extracted single slabs of varying thickness to minimise artefacts from hyper-reflective glial alterations found immediately below the ILM. They averaged pixels from 24 to 52μm below the ILM in the ONH area, from 24 to 36μm in the region between ONH and fovea and lastly reduced the sampled depths to 16-24μm in the temporal macula/raphe area. Although the approach retrieved a large proportion of reflectivity defects, it was possible to identify all RNFB lesions when the inspection was extended beyond 52μm below the ILM and generalised loss was considered.[10] In a study exploring the structure-function relationship in the macula of eyes with advanced glaucoma, Sakamoto et al[12] used 50μm fixed-thickness slabs from the ILM. The authors argued that the adopted axial depth would include approximately 20μm from the ganglion cell layer beneath a thinned RNFL but that this would be unlikely to alter reflectance results due to the hypo-reflectance of the ganglion cell layer.[12]

Using a fixed depth slab to sample regions of the retina with different RNFL thickness may fail to capture all glaucomatous defects. While often included as a limitation, most studies using enface OCT imaging in glaucoma have not accounted for differences

between retinal regions, nor between different eyes.[10-12,14] According to our data, the conventional 50μm thick slab might only be inclusive of all RNFBs in a limited number of retinal regions. In the nasal macula, the superior/inferior central retina and the ONH region, information regarding the status of bundles might be overlooked by this approach (Figure 3), as shown in one previous report.[10] Further, such methods would likely exceed the RNFL in its thinner regions, resulting in the inclusion of deeper, hypo-reflective retinal layers. Consequently, the observed lower intensities of RNFBs could arise not only because of a primary loss of reflectivity but also from the inclusion of deeper layers in the slab. As such, the ability to identify enface defects may vary according to slab thickness and composition. Since RNFBs are visible at different depths in different areas of the retina, slab thickness should also vary across the retina to include a consistent proportion of the RNFL.

It has been suggested that glaucomatous RNFL defects observed as loss of reflectivity might not necessarily be matched by a reduction in thickness.[11,41] Reflectivity defects may, therefore, provide additional information on RNFL status in glaucoma.[41,42] Disagreement between these two approaches might have several sources, including the method used to generate data. Indeed, thickness analysis relies fully on segmentation which is sometimes inaccurate, especially for the proximal RNFL boundary.[11] Conversely, enface imaging depends only on the vitreous-ILM segmentation, possibly the easiest surface to automatically detect.[44] Additionally, and perhaps more importantly, current enface images provide a combination of RNFL thickness and intensity, which might show evidence of glaucoma lesions on a different timescale.[8,11,15] Despite possible disagreement in glaucoma, RNFL thickness and the range of depths across which bundles are visible were highly correlated in the healthy eyes assessed in this study (Figure 6). This strong correlation provides face validity that the graders' subjective ratings were indeed based on visible RNFBs, supporting the clinical relevance of the technique. Although highly correlated, the slope of the points in the scatterplot is below the 1:1 line, suggesting that the range of depths across which bundles are visible overestimates RNFL thickness. This overestimate is likely to be an artefact of our instructions to graders; bundles were considered to be visible when occupying more than 25% of the region. This could have led to incongruences with the RNFL thickness, calculated as the mean across the region,

which may be more likely to represent the depth with visible bundles in 50% of the region.

Several limitations of this study require consideration. Firstly, only a small number of healthy eyes, of a single ethnic group (9/10 participants were Caucasian), were imaged. Although this provided adequate power to assess agreement among graders, it is possible that some more unusual RNFL configurations or thicknesses may not be captured in our sample. Similarly, the opportunistic selection of a small number of eyes may limit generalisability to different populations or settings. Nonetheless, the included age group was selected to be similar to that of open angle glaucoma,[28] limiting the impact of healthy ageing on the applicability of our findings.

Previous work considered raw OCT intensities to explore reflectivity defects of the RNFL,[7] yet, the overall incident light strength, media quality and age were reported to affect measurements.[42,45-47] To account for the variable amount of incident light, pixel intensity can be normalised to that of a reference layer.[41,42,48] Alternatively, as in our study, depth-resolved attenuation coefficients can be used to determine intrinsic optical properties of retinal tissue independent of the amount of light received as well as of additional segmentation requirements.[30,31,49] Whilst this method is expected to reduce artefacts, one study suggested that age and scan quality may still have a significant effect on attenuation coefficients.[49] In this study, these effects were likely to be minimised by the qualitative nature of the grading task, the inclusion of subjects only within the age range of interest and the inclusion only of scans well above the manufacturer's recommended minimum quality.

Finally, the image processing methods applied in our work have some drawbacks. For instance, as proposed elsewhere[10] we accounted for background intensity of individual images by extracting the value in the raphe region. However, this relies on the assumption of constant background throughout the whole retina which may not necessary hold for all participants. Further, scan montaging software was not available at the time of analysis. In the pseudo-montaged images used, overlapping areas of adjacent images were obscured by greyish masks for display (Figure 2) and clinicians were invited to ignore those regions while assessing RNFB visibility. Whist this method of displaying the images represents a compromise between maintaining positional context of the individual images and avoiding duplication of information and

registration errors, the graders were able to overcome the drawbacks to produce highly consistent and repeatable data. As such we do not believe the results of this study would be significantly altered by improved montaging of the individual images.

Due to the moving ILM reference plane with RNFL thinning in glaucoma, further work is needed to fully assess the slab properties required to fully capture RNFB defects in glaucoma. For example, whilst 50 μm below the ILM may be well within the RNFL of a healthy retina close to the optic disc, it may be within the ganglion cell layer of a glaucomatous retina with significant RNFL thinning. Nevertheless, our data suggest that it is possible that the fixed-slab approaches taken in previous studies may not fully capture all defects in early glaucoma. The data presented here provide preliminary evidence on the range of depths that should be considered by studies using enface OCT imaging in glaucoma.

In conclusion, the range of depths with visible RNFBs varied markedly across the retina of the healthy participants in this study, consistent with the RNFL thickness. The optimal single depth for visualisation of RNFBs across healthy retinae examined was around 20μm below the ILM. At this depth a cross section of the RNFB pattern was visible in all retinal regions and future work could explore whether these parameters would remain similar in a larger population or in different ethnic groups. To fully extract all RNFB information consistently across the retina, slab properties should account for changes in retinal location and differences between individual eyes should be considered.

References

1.   Tatham AJ, Medeiros FA, Zangwill LM & Weinreb RN. Strategies to improve early diagnosis in glaucoma. Progress in brain research. 2015;221:103-33.
2.   Chen TC, Hoguet A, Junk AK, et al. Spectral-Domain OCT: Helping the Clinician Diagnose Glaucoma: A Report by the American Academy of Ophthalmology. Ophthalmology. 2018;125(11):1817-27.
3.   Fallon M, Valero O, Pazos M & Anton A. Diagnostic accuracy of imaging devices in glaucoma: A meta-analysis. Survey of ophthalmology. 2017;62(4):446-61.
4.   de Moraes CG, Liebmann JM, Medeiros FA & Weinreb RN. Management of advanced glaucoma: Characterization and monitoring. Survey of ophthalmology. 2016;61(5):597-615.
5.   Kansal V, Armstrong JJ, Pintwala R & Hutnik C. Optical coherence tomography for glaucoma diagnosis: An evidence based meta-analysis. PloS one. 2018;13(1):e0190621.
6.   World Glaucoma Association. 10th Consensus Meeting: Diagnosis of Primary Open Angle Glaucoma. R.N. Weinreb, D.F. Garway-Heath, C. Leung, F.A. Medeiros, Liebmann J, editors2016.

7.   Vermeer KA, Schoot Jvd, Lemij HG & Boer JFd. OCT-derived Retinal Nerve Fiber Layer Reflectivity Maps for Glaucoma Assessment. Investigative ophthalmology & visual science. 2011;52(14):3666-.

8.   Liu S, Wang B, Yin B, et al. Retinal nerve fiber layer reflectance for early glaucoma diagnosis. Journal of glaucoma. 2014;23(1):e45-52.

9.   Huang XR, Knighton RW & Cavuoto LN. Microtubule contribution to the reflectance of the retinal nerve fiber layer. Investigative ophthalmology & visual science. 2006;47(12):5363-7.

10.   Ashimatey BS, King BJ, Burns SA & Swanson WH. Evaluating glaucomatous abnormality in peripapillary optical coherence tomography enface visualisation of the retinal nerve fibre layer reflectance. Ophthalmic & physiological optics : the journal of the British College of Ophthalmic Opticians (Optometrists). 2018;38(4):376-88.

11.   Hood DC, Fortune B, Mavrommatis MA, et al. Details of Glaucomatous Damage Are Better Seen on OCT En Face Images Than on OCT Retinal Nerve Fiber Layer Thickness Maps. Investigative ophthalmology & visual science. 2015;56(11):6208-16.

12.   Sakamoto M, Mori S, Ueda K, et al. En Face Slab Images Visualize Nerve Fibers With Residual Visual Sensitivity in Significantly Thinned Macular Areas of Advanced Glaucomatous Eyes. Investigative ophthalmology & visual science. 2019;60(8):2811-21.

13.   Huang XR, Knighton RW, Spector YZ & Feuer WJ. Cytoskeletal Alteration and Change of Retinal Nerve Fiber Layer Birefringence in Hypertensive Retina. Current eye research. 2017;42(6):936-47.

14.   Iikawa R, Togano T, Sakaue Y, et al. Estimation of the central 10-degree visual field using en-face images obtained by optical coherence tomography. PloS one. 2020;15(3):e0229867.

15.   Huang XR, Zhou Y, Kong W & Knighton RW. Reflectance decreases before thickness changes in the retinal nerve fiber layer in glaucomatous retinas. Investigative ophthalmology & visual science. 2011;52(9):6737-42.

16.   Malik R, Swanson WH & Garway-Heath DF. 'Structure-function relationship' in glaucoma: past thinking and current concepts. Clinical & experimental ophthalmology. 2012;40(4):369-80.

17.   Shigueoka LS, Vasconcellos JPC, Schimiti RB, et al. Automated algorithms combining structure and function outperform general ophthalmologists in diagnosing glaucoma. PloS one. 2018;13(12):e0207784.

18.   Raza AS, Zhang X, De Moraes CG, et al. Improving glaucoma detection using spatially correspondent clusters of damage and by combining standard automated perimetry and optical coherence tomography. Investigative ophthalmology & visual science. 2014;55(1):612-24.

19.   Hood DC, Tsamis E, Bommakanti NK, et al. Structure-Function Agreement Is Better Than Commonly Thought in Eyes With Early Glaucoma. Investigative ophthalmology & visual science. 2019;60(13):4241-8.

20.   Denniss J, Turpin A & McKendrick AM. Relating optical coherence tomography to visual fields in glaucoma: structure-function mapping, limitations and future applications. Clinical & experimental optometry. 2018.

21.   Denniss J, McKendrick AM & Turpin A. Towards Patient-Tailored Perimetry: Automated Perimetry Can Be Improved by Seeding Procedures With Patient-Specific Structural Information. Translational vision science & technology. 2013;2(4):3.

22.   Montesano G, Rossetti LM, Allegrini D, Romano MR & Crabb DP. Improving Visual Field Examination of the Macula Using Structural Information. Translational vision science & technology. 2018;7(6):36.

23.   Ganeshrao SB, McKendrick AM, Denniss J & Turpin A. A perimetric test procedure that uses structural information. Optometry and vision science : official publication of the American Academy of Optometry. 2015;92(1):70-82.

24.   Ballae Ganeshrao S, Turpin A & McKendrick AM. Sampling the Visual Field Based on Individual Retinal Nerve Fiber Layer Thickness Profile. Investigative ophthalmology & visual science. 2018;59(2):1066-74.

25.   Alluwimi MS, Swanson WH, Malinovsky VE & King BJ. A basis for customising perimetric locations within the macula in glaucoma. Ophthalmic & physiological optics : the journal of the British College of Ophthalmic Opticians (Optometrists). 2018;38(2):164-73.

26.   Alluwimi MS, Swanson WH, Malinovsky VE & King BJ. Customizing Perimetric Locations Based on En Face Images of Retinal Nerve Fiber Bundles With Glaucomatous Damage. Translational vision science & technology. 2018;7(2):5.

27.   Varma R, Skaf M & Barron E. Retinal nerve fiber layer thickness in normal human eyes. Ophthalmology. 1996;103(12):2114-9.

28.   Rudnicka AR, Mt-Isa S, Owen CG, Cook DG & Ashby D. Variations in primary open-angle glaucoma prevalence by age, gender, and race: a Bayesian meta-analysis. Investigative ophthalmology & visual science. 2006;47(10):4254-61.

29.   Ctori I & Huntjens B. Repeatability of Foveal Measurements Using Spectralis Optical Coherence Tomography Segmentation Software. PloS one. 2015;10(6):e0129005.

30.   Vermeer KA, Mo J, Weda JJ, Lemij HG & de Boer JF. Depth-resolved model-based reconstruction of attenuation coefficients in optical coherence tomography. Biomedical optics express. 2013;5(1):322-37.

31.   Chang S & Bowden AK. Review of methods and applications of attenuation coefficient measurements with optical coherence tomography. Journal of biomedical optics. 2019;24(9):1-17.

32.   R Core Team. R: A language and environment for statistical computing. R version 3.6.3 (2020-02-29) ed: R Foundation for Statistical Computing, Vienna, Austria; 2020.

33.   Bedggood P, Nguyen B, Lakkis G, Turpin A & McKendrick AM. Orientation of the Temporal Nerve Fiber Raphe in Healthy and in Glaucomatous Eyes. Investigative ophthalmology & visual science. 2017;58(10):4211-7.

34.   Denniss J, McKendrick AM & Turpin A. An anatomically customizable computational model relating the visual field to the optic nerve head in individual eyes. Investigative ophthalmology & visual science. 2012;53(11):6981-90.

35.   Ashimatey BS, King BJ & Swanson WH. Retinal putative glial alterations: implication for glaucoma care. Ophthalmic & physiological optics : the journal of the British College of Ophthalmic Opticians (Optometrists). 2018;38(1):56-65.

36.   Bates D, Mächler M, Bolker B & Walker SJapa. Fitting linear mixed-effects models using lme4. 2014.

37.   Shrout PE & Fleiss JL. Intraclass correlations: uses in assessing rater reliability. Psychological bulletin. 1979;86(2):420-8.

38.   Revelle W. psych: Procedures for Personality and Psychological Research, Northwestern University, Evanston, Illinois, USA 2018 [

39.   Finn RH. A note on estimating the reliability of categorical data. Educational Psychological Measurement. 1970;30(1):71-6.

40.   Denniss J, Turpin A, Tanabe F, Matsumoto C & McKendrick AM. Structure-function mapping: variability and conviction in tracing retinal nerve fiber bundles and comparison to a computational model. Investigative ophthalmology & visual science. 2014;55(2):728-36.

41.   Gardiner SK, Demirel S, Reynaud J & Fortune B. Changes in Retinal Nerve Fiber Layer Reflectance Intensity as a Predictor of Functional Progression in Glaucoma. Investigative ophthalmology & visual science. 2016;57(3):1221-7.

42.   Vermeer KA, van der Schoot J, Lemij HG, de Boer JFJIo & science v. RPE-normalized RNFL attenuation coefficient maps derived from volumetric OCT imaging for glaucoma assessment. 2012;53(10):6102-8.

43.   Hondur G, Goktas E, Al-Aswad L & Tezel G. Age-related changes in the peripheral retinal nerve fiber layer thickness. Clinical ophthalmology (Auckland, NZ). 2018;12:401-9.

44.   Yang Q, Reisman CA, Wang Z, et al. Automated layer segmentation of macular OCT images using dual-scale gradient information. Optics express. 2010;18(20):21293-307.

45.   Chen X, Hou P, Jin C, et al. Quantitative analysis of retinal layer optical intensities on three-dimensional optical coherence tomography. Investigative ophthalmology & visual science. 2013;54(10):6846-51.

46.   Tappeiner C, Barthelmes D, Abegg MH, Wolf S & Fleischhauer JC. Impact of optic media opacities and image compression on quantitative analysis of optical coherence tomography. Investigative ophthalmology & visual science. 2008;49(4):1609-14.

47.   Chen B, Gao E, Chen H, et al. Profile and Determinants of Retinal Optical Intensity in Normal Eyes with Spectral Domain Optical Coherence Tomography. PloS one. 2016;11(2):e0148183.

48.   Mehta N, Lavinsky F, Gattoussi S, et al. Increased Inner Retinal Layer Reflectivity in Eyes With Acute CRVO Correlates With Worse Visual Outcomes at 12 Months. Investigative ophthalmology & visual science. 2018;59(8):3503-10.

49.   Thepass G, Lemij HG & Vermeer KA. Attenuation Coefficients From SD-OCT Data: Structural Information Beyond Morphology on RNFL Integrity in Glaucoma. Journal of glaucoma. 2017;26(11):1001-9.